RSC Advances

PAPER

View Article Online
View Journal | View Issue

Cite this: RSC Adv., 2017, 7, 1540

Structure and thermal properties of millimeter-scale alumina aerogel beads formed by a modified ball dropping method

Yuxi Yu,*[a] Mengwei Zhu[a] and Jiyu Fang[b]

Received 10th November 2016
Accepted 19th December 2016

DOI: 10.1039/c6ra26601k

www.rsc.org/advances

We report the formation of millimeter-sized alumina aerogel beads with a modified ball dropping method, in which alumina alcogel beads are formed by extruding an alumina sol containing a small amount of polyvinyl alcohol (PVA) through nozzles into ammonia water, followed by supercritical drying. The resultant millimeter-sized alumina aerogel beads with the diameter ranging between 1–4 mm have an average pore size of 12–14 nm and specific surface area of 500–600 $m^2\ g^{-1}$. They transform from γ-AlO_2H phase to γ-Al_2O_3 phase at 400 °C, which remains stable even when the temperature reaches 1200 °C.

1. Introduction

Alumina is a well-known fine ceramic material with good thermal, chemical, and mechanical stability.[1] Aerogels are attractive due to their large surface area, high porosity and low density.[2] Recently, there has been interest in the synthesis of alumina aerogels because of their potential applications as catalytic substrates, porous membranes, and thermal insulators.[3–5] The sol–gel reaction coupled with the supercritical drying process is a common method for the synthesis of alumina aerogels.[6,7] So far, most alumina aerogels reported in the literature are monolithic with varied sizes and shapes.[4] Compared monolithic aerogels, aerogel beads are more suitable in energy and biomedical applications because they can be easily packed in devices and uptaken by biological cells. Great efforts have been made in the synthesis of aerogel beads.[8–12] For example, Yun *et al.*[11] reported the synthesis of silica aerogel microspheres using a emulsion method. However, the method cannot be used for synthesizing millimeter-sized aerogel beads. Sarawade *et al.*[13] developed a ball-dropping method for the synthesis of millimeter-sized silica aerogel beads. Previously, we prepared millimeter-sized silica–titania[14] aerogel beads by the facile ball-dropping method, followed by supercritical drying. However, millimeter-sized alumina aerogel beads cannot be directly formed from with the ball dropping method.

In this paper, we modify the ball dropping method to prepare millimeter-sized alumina aerogel beads, in which alumina alcogel beads are generated by extruding alumina sol containing a small amount of polyvinyl alcohol (PVA) through nozzles into ammonia water, followed by supercritical drying process. The resultant alumina aerogel beads have diameters in the range from 1 mm to 4 mm with the average pore size of 12–14 nm and the specific surface area of 500–600 $m^2\ g^{-1}$. They transform from γ-AlO_2H boehmite phase to γ-Al_2O_3 phase at 400 °C, which remains stable even when the temperature reaches to 1200 °C.

2. Materials and methods

2.1 Materials

Aluminum isopropoxide (AIP), ethyl acetoacetate (Etac), polyvinyl alcohol (PVA) and ethanol (EtOH) with a purity of 99% were purchased from Sinopharm Chemical Reagent Co. Ltd. Deionized water (H_2O, 18 ΩM and pH 5.7) was from an ion exchange system. Nitric acid (HNO_3) was purchased from Xilong Chemical Co. Ltd.

2.2 Synthesis of alumina aerogel beads

Fig. 1 shows the schematic representation of the synthesis process of alumina aerogel beads. Briefly, AIP, EtOH, Etac and H_2O were mixed in a beaker and then stirred for 60 min at 75 °C, followed by the addition of HNO_3 to form alumina sol. The molar ratio of the mixture is 1 mol AIP : 9 mol EtOH : 0.3 mol Etac : 45 mol H_2O : 0.3 mol HNO_3. PVA solution was prepared by stirring PVA in deionized water at 90 °C for 2 h. Alumina sol was then mixed with PVA solution at different ratios. The alumina gel beads were formed by extruding alumina sol though a nozzle with different inner diameters into a vessel containing kerosene as an upper layer and ammonia water as a down layer. The sol–gel reaction started when alumina sol droplets with PVA contacted with ammonia water. The resultant

[a]Department of Materials Science and Engineering, College of Materials, Fujian Key Laboratory of Advanced Materials, Xiamen University, Xiamen 361005, China. E-mail: yu_heart@xmu.edu.cn

[b]Department of Materials Science and Engineering, Advanced Materials Processing and Analysis Center, University of Central Florida, Orlando, Florida 32816, USA

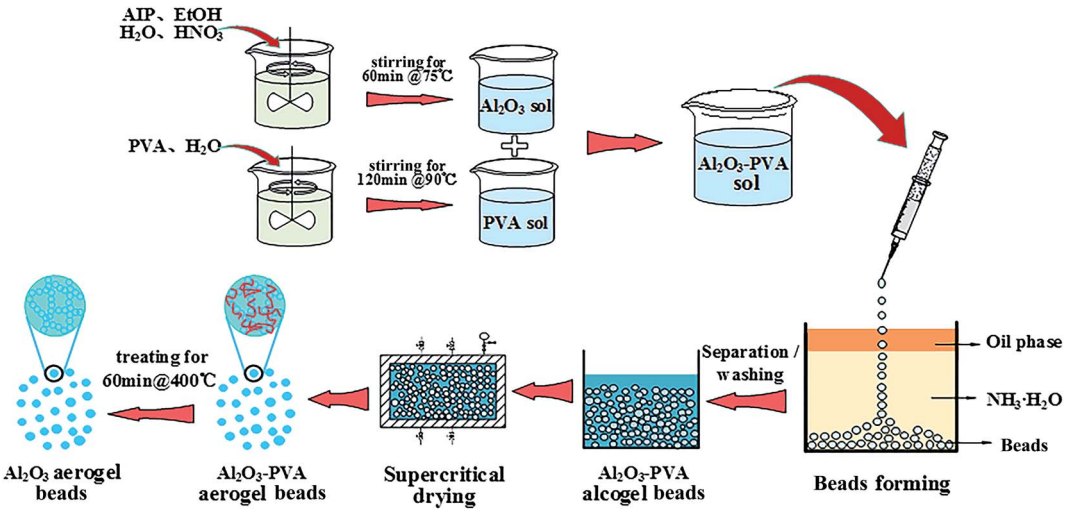

Fig. 1 Schematic representation of the synthesis process of alumina aerogel beads.

gel beads were immerged in ammonia water for 2 h, followed by washing with alcohol and then were immersed in alcohol. Finally, the alumina aerogel beads were obtained by ethanol supercritical drying (260 °C and 12 MPa).

2.3 Characterization methods

The bulk density ($\rho = m/v$) of alumina aerogel beads was calculated based on their mass (m) to volume (v) ratios. The crystalline structure of alumina aerogel beads was measured by X-ray diffraction (XRD, X'pert PRO, PANalytical, Netherlands) with CuK radiation ($\lambda = 1.542$ Å). For the XRD measurement, alumina aerogel beads were ground into powders and then planished into a sheet on a glass substrate. The microstructure of alumina aerogel beads were characterized with a scanning electron microscope (SEM, SU-70, Hitachi High-Tech, Japan) at 10 kV and a transmission electron microscope (TEM, JEM-2100, JEOL, Japan) at 200 kV. For the SEM measurement, the powder from alumina aerogel beads was placed on a conducting resin and then coated with gold. For TEM measurements, the powders were placed on a copper wire mesh. The thermal analysis was conducted by thermo gravimetric analysis (TGA/DTA, STA 449 F3 Jupiter, Netzsch, Germany) from room temperature to 1200 °C with a rate of 10 °C min^{-1} under air flow. Fourier transform infrared spectroscopy (FT-IR, Avatar 360, Nicolet IN10, USA) was used to measure the chemical bonding of alumina aerogel beads in transmittance mode. The surface area and pore size distribution of alumina aerogel beads were analyzed by nitrogen gas adsorption and desorption method (TriStar II 3020, Micromeritics, USA). The nitrogen adsorption and desorption curves were measured at the temperature of liquid nitrogen (−196 °C) using Micromeritics Tristar II 3020. Before the nitrogen adsorption, alumina aerogel beads were degassed at 200 °C for 4 h. The surface area and pore size distribution of alumina aerogel beads were obtained with Brunauer–Emmett–Teller (BET) and Barrett–Joyner–Halenda (BJH) methods, respectively.

3. Results and discussion

3.1 Synthesis and morphology of alumina aerogel beads

The formation of alumina alcogel beads is prerequisite for the synthesis of alumina aerogel beads. However, alumina sol cannot be directly transformed into alumina alcogel beads with the ball dropping method easily for the rapid coagulating phenomenon with lower strength at the same time (Fig. 2a). We find that the addition of a small amount of PVA (0.5 wt% to 2 wt%) in alumina sol can form the shape of alcogel beads from the oil phase easily for the stabilization of PVA. As we know, the PVA has many hydroxyl groups on structure, they can help to increase the possibility of the adhesive with the hydrolysis AIP alumina sol and improve the hydrogen bonding interaction. We also find the degree of sphericity is improved with the increase of PVA, especially from 0.5 wt% to 1 wt% (Fig. 2b and c), this is because the PVA can increase the viscosity of the sol and the shape of bead can be held steady without deformation. From the optical images of alumina aerogel beads (Fig. 2b1 and e1), we can see clearly that the color of the beads is deepen with the increase of PVA, that is easy to understand for the more PVA, the more oxidation of hydroxyl groups and production more residues. The nitrogen gas adsorption and desorption were made to get more information in Table 1, but we cannot see obvious differences between these samples except a little increase in average pore size and pore volume.

We should know that the size of nozzle has an effect on the final alcohol beads. In order to study and verify the effect, we used the single nozzle by different nozzle apertures to prepare the alumina alcogel beads containing 1 wt% PVA, the diameters of nozzles are 0.33 mm, 0.41 mm, 0.72 mm and 0.91 mm, respectively. Optical images of alumina alcogel beads are shown in Fig. 3. The results show that there is distinct difference between the sizes of alcogel beads ranging from 1 mm to 4 mm under different nozzle sizes. As we can know, the bigger nozzle size will generate the larger tractive force from the nozzle, and there will be greater gravity force to overcome the tractive force

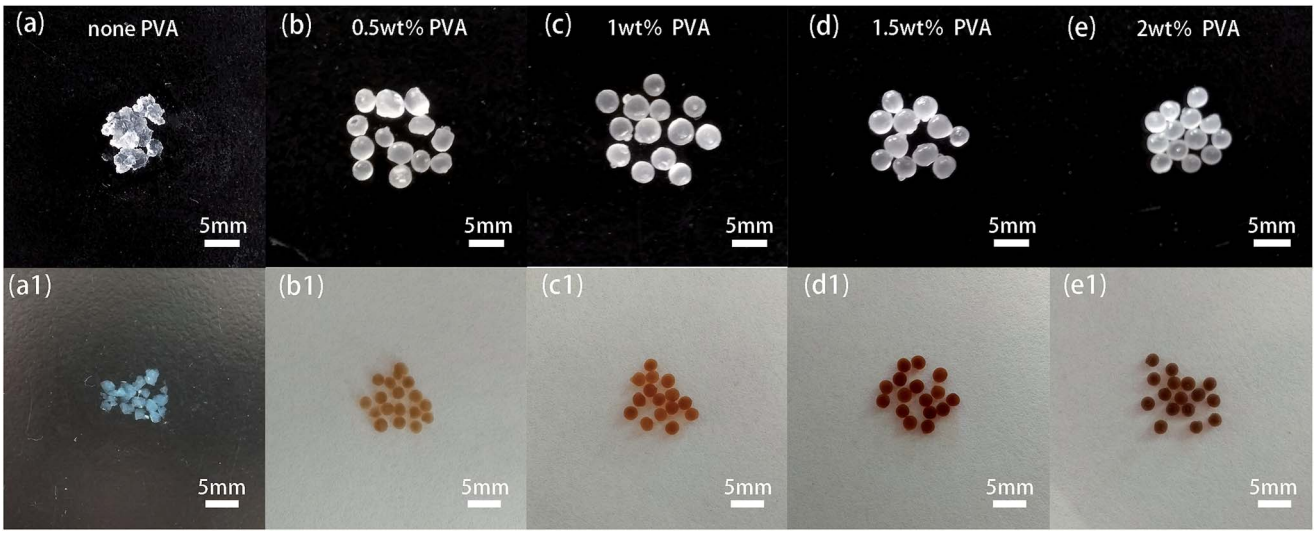

Fig. 2 Optical images of alumina alcogel beads (a–e) and alumina aerogel beads (a1–e1) prepared with different contents of PVA.

Table 1 Information of alumina aerogel beads with different contents of PVA

Samples	Specific surface area ($m^2\ g^{-1}$)	Average pore size (nm)	Average particle size (nm)	Pore volume ($cm^3\ g^{-1}$)
None PVA	530.34	12.19	11.31	1.570
0.5 wt% PVA	530.59	13.52	11.30	1.702
1 wt% PVA	586.95	12.22	10.22	1.765
1.5 wt% PVA	586.73	13.60	10.22	1.962
2 wt% PVA	572.57	14.60	10.47	2.022

for detaching from the nozzle, which means the greater liquid volume of alumina sol, so this makes the bigger alcogel beads finally. This result proves our conjecture and helps us choose the appropriate nozzle to get the beads we want.

Fig. 4a shows the photograph of alumina alcogel beads formed from alumina sol with 1 wt% PVA though a nozzle with a diameter of 0.41 mm. After the supercritical drying at 260 °C and 12 MPa, alumina alcogel beads transfer into aerogel beads, which have spherical shape with the diameter of 2.0 ± 0.5 mm in brown color (Fig. 4b). It can be seen in the SEM image shown in Fig. 4c that alumina aerogel beads consist of nanoparticles which interconnect into a three-dimensional mesoporous network. The TEM image shows the as-prepared alumina alcogel bead exhibits randomly interconnected networks consisted of nanometer-sized needle-like particles with thickness of 1–3 nm and length of 20–40 nm (Fig. 4d).[5]

3.2 Thermal properties of alumina aerogel beads

The thermostability of alumina aerogel beads was evaluated through the thermal treatment at 400 °C, 500 °C,800 °C,

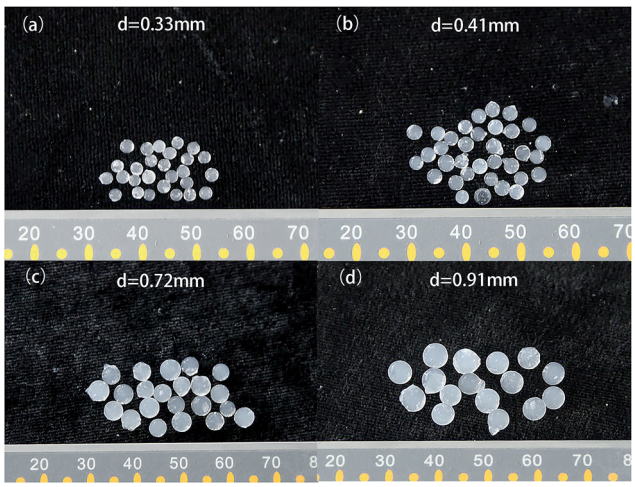

Fig. 3 Optical images of alumina alcogel beads prepared by different nozzle sizes (a) $d = 0.31$ mm, (b) $d = 0.41$ mm, (c) $d = 0.72$ mm, (d) $d = 0.91$ mm.

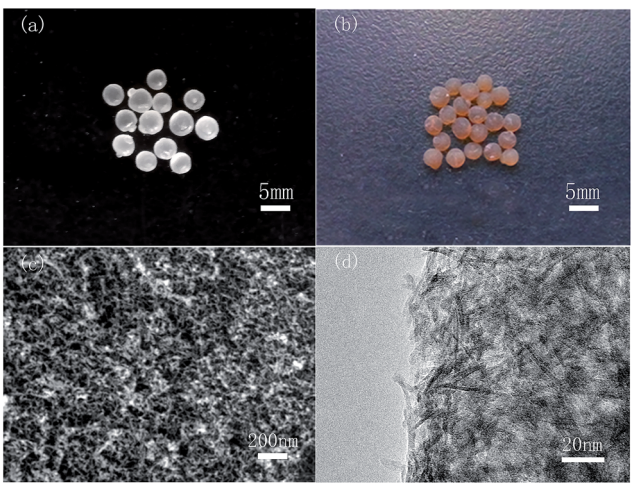

Fig. 4 Photographs of alumina alcogel beads (a); alumina aerogel beads (b); SEM image (c) and TEM image (d) of alumina aerogel beads containing 1 wt% PVA though a nozzle size of 0.41 mm.

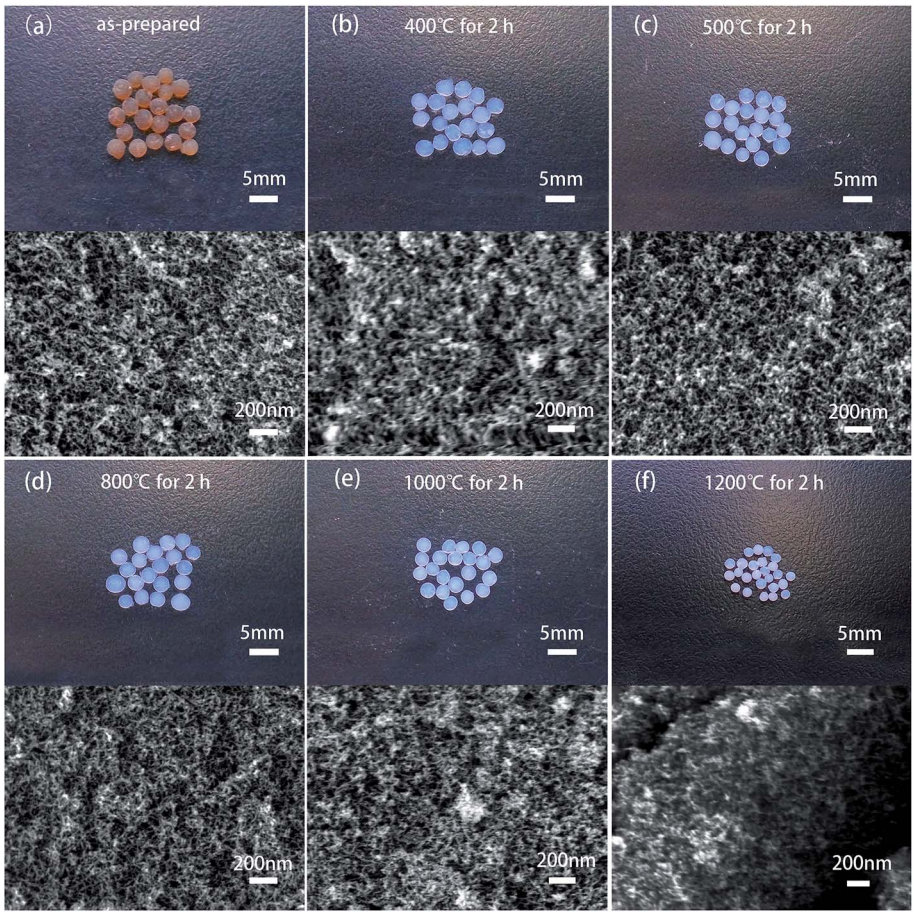

Fig. 5 Photographs of alumina aerogel beads containing 1 wt% PVA before and after the thermostreatment at different temperatures. The corresponding SEM images are below.

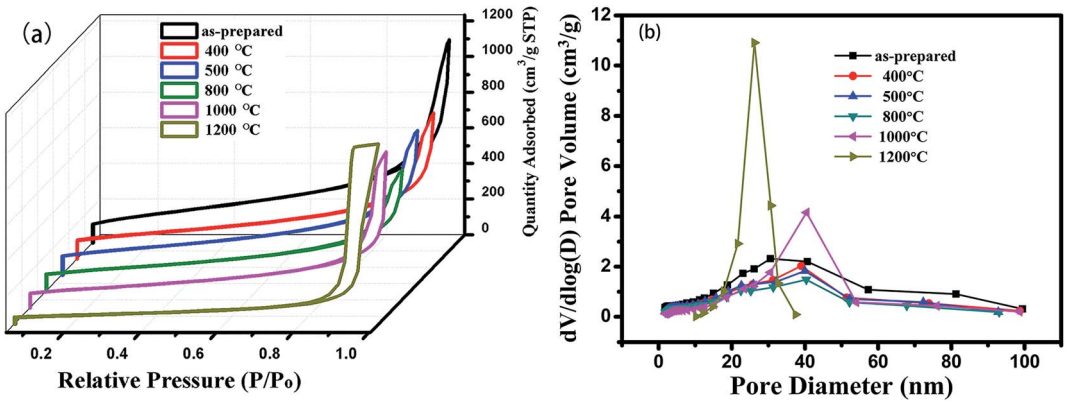

Fig. 6 (a) N_2 nitrogen adsorption–desorption isotherms and (b) pore size distributions of alumina aerogel beads thermotreated at different temperatures for 2 h.

1000 °C, and 1200 °C for 2 h, respectively. Fig. 5 shows the photograph of the alumina aerogel beads before and after the thermal treatment. Brown alumina aerogel beads become transparent after the 2 h thermal treatment at 400 °C due to the decomposition of PVA (Fig. 5a and b). The size of alumina aerogel beads remains unchanged until the temperature of the thermal treatment reaches to 1200 °C (Fig. 5c and e). After the thermal treatment at 1200 °C for 2 h, alumina aerogel beads shrink ~40% in their sizes (Fig. 5f). Furthermore, the densification of nanoparticles in alumina aerogel beads after the thermal treatment at 1200 °C are clearly visible from the corresponding SEM images below in Fig. 5.

Table 2 Information of alumina aerogel beads containing 1 wt% PVA before and after the thermostreatment at different temperatures

Samples	Specific surface area ($m^2\ g^{-1}$)	Average pore size (nm)	Bulk density ($g\ cm^{-3}$)
As-prepared	586.95	12.12	0.120
400 °C	502.42	12.38	0.121
500 °C	479.92	11.67	0.125
800 °C	433.00	11.76	0.134
1000 °C	376.56	16.88	0.153
1200 °C	171.99	24.58	0.584

The porosity of these thermo-threated alumina aerogel beads is studied by nitrogen adsorption–desorption measurements, which shows the type-IV isotherms with type H1 hysteresis loops (Fig. 6a). The alumina aerogel beads containing 1 wt% PVA adsorb the maximum amount of saturated N_2 gas at the relative pressure of 0.99. The pore size distribution of alumina aerogel beads calculated with Barrett–Joyner–Halenda (BJH) method is shown in Fig. 6b. There is no significant change in the average pore size of alumina aerogel beads until the temperature reaches to 1000 °C (Table 2). Beyond that, a relatively large change in the average pore size is observed when the temperature reaches to 1200 °C. The specific surface area of alumina aerogel beads calculated with Brunauer–Emmett–Teller (BET) method shows gradual decreases from 586.95 $m^2\ g^{-1}$ to 171.99 $m^2\ g^{-1}$ when the increase increases from 25 °C to 1200 °C (Table 2). The change in the bulk density of alumina aerogel beads as a function of temperature is also shown in Table 2.

Fig. 7 is the TG-DTA curves of alumina aerogel beads. The TG curve shows that there are two weight losses. The first weight loss (~3.15%) occurs within 100 °C, which is attributed to the volatilization of water and ethanol. The second weight loss (~16.73%) takes place in the temperature range from 300 to 600 °C. The DTA curve shows an endothermic peak at 250 °C, which corresponds to the removal of constitution water ($2AlO_2H = Al_2O_3 + H_2O\uparrow$).[15] In the temperature range from 300 to 600 °C, we observe a broad exothermic peak in the DTA curve, due to the oxygen lysis process of the incomplete hydrolysis of $-OCH(CH_3)_2$ groups and the transformation from the boehmite γ-AlO_2H phase to γ-Al_2O_3 phase.[16] There is no further weight loss and exothermic peak observed from 800 °C to 1200 °C, suggesting that alumina aerogel beads have good thermal stability in this temperature range.

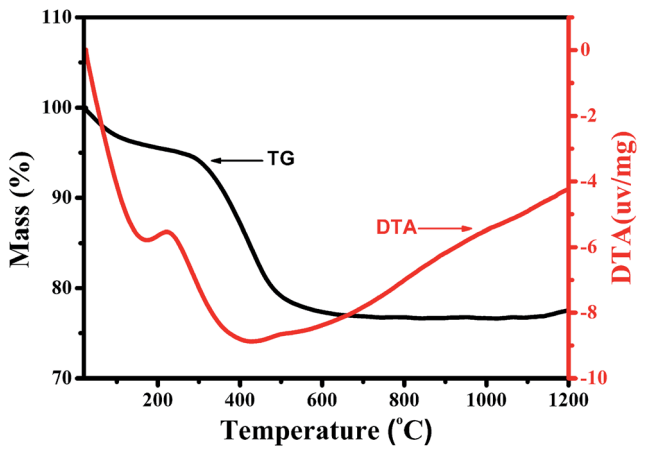

Fig. 7 TG-DTA curves of alumina aerogel beads containing 1 wt% PVA.

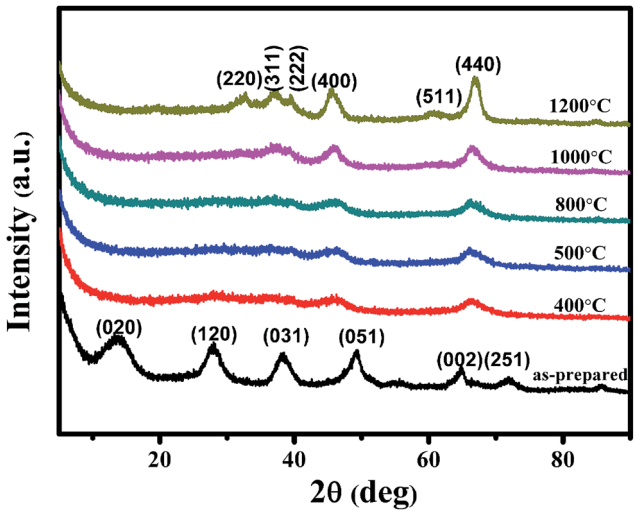

Fig. 8 XRD patterns of alumina aerogel beads containing 1 wt% PVA treated at different.

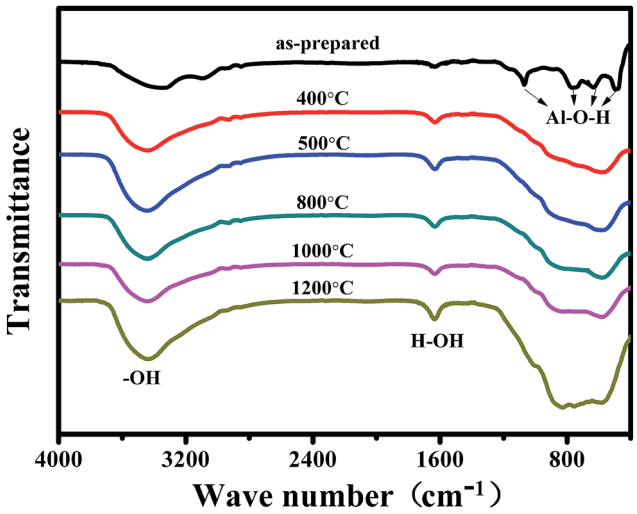

Fig. 9 FT-IR curves of alumina aerogel beads containing 1 wt% PVA treated at different temperatures for 2 h.

Fig. 8 shows the X-ray diffraction patterns of alumina aerogel beads containing 1 wt% PVA before and after the thermal treatment at different temperatures. Before the thermal treatment, the alumina aerogel beads show the six diffraction peaks from the scattering from the (020), (120), (031), (051), (002) and (251) planes of boehmite γ-AlO_2H phase (JCPDS card 49-0133).[17,18] After the thermal treatment, we observe the six diffraction peaks from the scattering from the (220), (311), (222), (400), (511) and (440) planes of γ-Al_2O_3 phase (JCPDS card

04-0875).[18] The intensity of the diffraction peaks increases with the increase of temperature. There is no transition from γ-Al_2O_3 phase to α-Al_2O_3 phase observed even when the temperature reaches to 1200 °C, suggesting that alumina aerogel beads are highly stable.

Fig. 9 shows the FT-IR spectra of alumina aerogel beads containing 1 wt% PVA before and after thermal treatment. Before the thermal treatment, the peak at 1065, 767, 635 and 488 cm^{-1} can be assigned to the Al–O–H vibrations of boehmite,[19] which vanishes after the thermal treatment. Instead, we observe a strong broad band in the range from 400 cm^{-1} to 1000 cm^{-1}, which is attributed to the Al–O vibration bond. The result indicates the γ-AlO_2H to γ-Al_2O_3 phase transformation takes place after the thermal treatment.

4. Conclusion

Millimeter-sized alumina aerogel beads have been successfully prepared by using a modified ball dropping method, in which alumina alcogel beads are formed by extruding alumina sol containing a small amount of PVA through nozzles into ammonia water, followed by supercritical drying. We find that the resultant millimeter-sized alumina aerogel beads with the diameter ranging between 1∼4 mm have the average pore size of 12–14 nm and the specific surface area of 500–600 $m^2\ g^{-1}$. They transform from γ-AlO_2H phase to γ-Al_2O_3 phase at 400 °C, which remains stable even when temperature reaches to 1200 °C. The thermally stable millimeter-sized alumina aerogel beads have great potential as adsorbents, catalytic supports, and templates to synthesize functional materials requiring high temperature resistance.

Acknowledgements

Financial support from the Natural Science Foundation of China (51675452) is acknowledged.

References

1 Z. Sun, B. Li, P. Hu, F. Ding and F. Yuan, *J. Alloys Compd.*, 2016, **688**, 933–938.
2 M. Koebel, A. Rigacci and P. Achard, *J. Sol-Gel Sci. Technol.*, 2012, **63**, 315–339.
3 M. Triki, Z. Ksibi, A. Ghorbel and F. Medina, *J. Sol-Gel Sci. Technol.*, 2011, **59**, 1–6.
4 F. Cao, L. Ren and X. Li, *RSC Adv.*, 2015, **5**, 18025–18028.
5 G. Q. Zu, J. Shen, L. P. Zou, W. Q. Wang, Y. Lian, Z. H. Zhang and A. Du, *Chem. Mater.*, 2013, **25**, 4757–4764.
6 Y. Mizushima and M. Hori, *J. Mater. Res.*, 1993, **8**, 2993–2999.
7 G. Zu, J. Shen, X. Wei, X. Ni, Z. Zhang, J. Wang and G. Liu, *J. Non-Cryst. Solids*, 2011, **357**, 2903–2906.
8 N. Dilsiz and G. Akovali, *Mater. Sci. Eng., A*, 2002, **332**, 91–96.
9 M. Alnaief and I. Smirnova, *J. Supercrit. Fluids*, 2011, **55**, 1118–1123.
10 P. B. Sarawade, D. V. Quang, A. Hilonga, S. J. Jeon and H. T. Kim, *Mater. Lett.*, 2012, **81**, 37–40.
11 S. Yun, H. J. Luo and Y. F. Gao, *RSC Adv.*, 2014, **4**, 4535–4542.
12 Y. X. Yu, D. Q. Guo and J. Y. Fang, *J. Porous Mater.*, 2015, **22**, 621–628.
13 P. B. Sarawade, J. K. Kim, A. Hilonga and H. T. Kim, *Solid State Sci.*, 2010, **12**, 911–918.
14 Y. Yu, M. Zhu, W. Liang, S. Rhodes and J. Fang, *RSC Adv.*, 2015, **5**, 72437–72443.
15 J. Wang, X. Bokhimi, A. Morales, O. Novaro, T. Lopez and R. Gomez, *J. Phys. Chem. B*, 1999, **103**, 299–303.
16 S. Keysar, G. E. Shter, Y. de Hazan, Y. Cohen and G. S. Grader, *Chem. Mater.*, 1997, **9**, 2464–2467.
17 T. F. Baumann, A. E. Gash, S. C. Chinn, A. M. Sawvel, R. S. Maxwell and J. H. Satcher, *Chem. Mater.*, 2005, **17**, 395–401.
18 G. Hayase, K. Nonomura, G. Hasegawa, K. Kanamori and K. Nakanishi, *Chem. Mater.*, 2015, **27**, 3–5.
19 D.-Y. Li, Y.-S. Lin, Y.-C. Li, D.-L. Shieh and J.-L. Lin, *Microporous Mesoporous Mater.*, 2008, **108**, 276–282.